ruhr.paD
UA Ruhr Zentrum für
partielle Differentialgleichungen

A Prange-Hellinger-Reissner type finite element formulation for small strain elasto-plasticity

J. Schröder, M. Igelbüscher, A. Schwarz and G. Starke

Preprint 2016-17

A Prange-Hellinger-Reissner type finite element formulation for small strain elasto-plasticity

Jörg Schröder, Maximilian Igelbüscher, Alexander Schwarz, Gerhard Starke*

Institut für Mechanik, Fakultät für Ingenieurwissenschaften / Abtl. Bauwissenschaften
Universität Duisburg-Essen, 45141 Essen, Universitätsstr. 15, Germany
e-mail: j.schroeder@uni-due.de, maximilian.igelbuescher@uni-due.de, alexander.schwarz@uni-due.de
phone: +49 201 183 2708, fax: +49 201 183 2680

*Fakultät für Mathematik
Universität Duisburg-Essen, 45127 Essen, Thea-Leymann-Straße 9, Germany
e-mail: gerhard.starke@uni-due.de, phone: +49 201 183 2339, fax: +49 201 183 2601

Highlights

- Mixed Prange-Hellinger-Reissner type variational functional
- Algorithmic consistent treatment of plane stress and plane strain
- Point-wise enforcement of constraints due to elasto-plasticity in contrast to the element-wise treatment proposed by Simo et al. [1989]

Abstract

In this contribution we propose a mixed variational formulation of the Prange-Hellinger-Reissner type for elasto-plasticity at small strains. Here, the displacements and the stresses are interpolated independently, which are balanced within the variational functional by the relation of the elastic strains and the partial derivative of the complementary stored energy with respect to the stresses. For the elasto-plastic material behavior a von Mises yield criterion is considered, where we restrict ourselves w.l.o.g. to linear isotropic hardening. In the proposed formulation we enforce the constraints arising from plasticity point-wise in contrast to the element-wise realization of the plastic return mapping algorithm suggested in Simo et al. [1989]. The performance of the new formulation is demonstrated by the analysis of several benchmark problems. Here, we compare the point-wise treatment of elasto-plasticity with the original element-wise formulation of Simo et al. [1989]. Furthermore, we derive an algorithmic consistent treatment for plane stress as well as for plane strain condition.

Keywords: mixed FEM, elasto-plasticity, Prange-Hellinger-Reissner type functional, algorithmic consistent treatment, plane stress and plane strain

1. Introduction

An important field in finite element design is the improvement of the element performance, which is influenced by the reliability, stability and solution quality. In the past decades, an enormous effort was addressed to the development on finite element methods based on the variational approach going back to Galerkin [1915], which are in general considering the approximation of one field, e.g. the displacements. Further developments also consider additional fields in the variational setup for example in Reissner [1950] (compare also the early works of Hellinger [1914] and Prange [1916]), an independent stress approximation is

applied in addition to the displacements. We refer this type of formulation, which is based on a complementary stored energy function, as Prange-Hellinger-Reissner formulation. A few years later, Hu [1955] and Washizu [1955] proposed independently a variational principle related to displacements, stresses and strains, based on the so-called Hu-Washizu functional. In the work of Fraeijs de Veubeke [1951], five variational principles are derived starting from a four-field approach, in which surface tractions are independently varied, in addition to the aforementioned fields.

In Galerkin and Hu-Washizu type variational formulations, an often used approach for isotropic elasto-plastic problems is the application of a radial return algorithm, which consist of an elastic predictor and a plastic corrector step, see e.g. Wilkins [1964], Simo [1998] and Simo and Hughes [1998]. Therein, the flow rule has to be enforced point-wise at each quadrature point. Using the Prange-Hellinger-Reissner variational principle, Simo et al. [1989] postulate that the flow rule must be enforced in a weak sense on element level. Furthermore, it is also possible (not necessary) to enforce the hardening law and consistency conditions in weak sense on element level.

Mixed formulations often result into saddle-point problems and therefore a major constraint of these approaches is the restriction to the so-called LBB-conditions, see Ladyzhenskaya [1969], Babuška [1973], Brezzi [1974], Boffi et al. [2013] and Auricchio et al. [2004]. Mathematical aspects concerning the mixed finite element formulation for elasticity based on the Prange-Hellinger-Reissner (PHR) principle are given in Arnold and Winther [2003], Auricchio et al. [2004], Lonsing and Verfürth [2004], Arnold et al. [2007], Boffi et al. [2009] and Cockburn et al. [2010]. Often a discontinuous stress approximation using a 5-parameter ansatz proposed by Pian and Sumihara [1984] is used. The advantages of this approach are characterized by a remarkable insensitivity to mesh distortion, locking free behavior for plane strain quasi-incompressible elasticity and superconvergent results for bending dominated problems, see e.g. Simo et al. [1989], Pian and Sumihara [1984], Chun et al. [2008] and Wriggers and Korelc [1996]. An investigation of an extended dual PHR formulation with additional fields for Lagrangian multiplier and infinitesimal rotation field by Klaas et al. [1995] have shown optimal convergence for displacements and stresses using the BDM element, see Brezzi et al. [1985]. Furthermore, an extension to small strain elasto-plasticity is derived by Schröder et al. [1997]. Analysis of the well-posedness and convergence of finite element approximations of the elasto-plastic problems are treated in detail in Han and Reddy [1995] and Reddy [1992].

In the presented work, we propose a Prange-Hellinger-Reissner variational functional for isotropic elasto-plasticity for plane strain and plane stress conditions. Our focus is on the variational formulation, corresponding discrete formulation and associated algorithm for treating elasto-plasticity. The interpolation of the displacements is done by standard linear Lagrangian ansatz functions and the discontinuous stresses are approximated by the 5-parameter ansatz of Pian and Sumihara [1984]. Here, we apply a point-wise enforcement of the flow rule, the hardening law and the consistency conditions. This is in contrast to the statement given in Simo et al. [1989], which postulates that the flow rule can no longer be evaluated independently at each Gauss point. The resulting mixed finite element formulation under plane stress conditions is compared with the same boundary value problems presented in Simo et al. [1989]. Here, the plane stress conditions follows directly from the formulation by the restriction to two dimensions. Furthermore, we demonstrate the performance of the plane strain algorithm analyzing a plate with circular inclusion. Therein, the plane strain condition is enforced by an incremental algorithmic treatment.

2 Formulation of PHR principle for elasto-plasticity

In the following we introduce the Prange-Hellinger-Reissner principle for elasto-plasticity at small strains. Let $\mathcal{B}$ be the body of interest parameterized in $\boldsymbol{x}$ with the boundary $\partial\mathcal{B}$, satisfying

$$\partial\mathcal{B} = \partial\mathcal{B}_u \cup \partial\mathcal{B}_t \quad \text{and} \quad \partial\mathcal{B}_u \cap \partial\mathcal{B}_t = \emptyset\,, \tag{1}$$

where $\partial\mathcal{B}_u$ denotes the displacement boundary and $\partial\mathcal{B}_t$ the stress boundary. The linear strain tensor $\boldsymbol{\varepsilon}$ is defined by the symmetric displacement gradient as

$$\boldsymbol{\varepsilon} := \nabla^s \boldsymbol{u} = \frac{1}{2}(\nabla\boldsymbol{u} + (\nabla\boldsymbol{u})^T)\,. \tag{2}$$

For the framework of elasto-plasticity at small strains, we make use of the additive split of the total strains into an elastic $\boldsymbol{\varepsilon}^e$ and plastic $\boldsymbol{\varepsilon}^p$ part, i.e.

$$\boldsymbol{\varepsilon} = \boldsymbol{\varepsilon}^e + \boldsymbol{\varepsilon}^p \quad \text{or equivalently} \quad \boldsymbol{\varepsilon}^e = \boldsymbol{\varepsilon} - \boldsymbol{\varepsilon}^p\,. \tag{3}$$

We first consider the potential energy functional, which is given by

$$\Pi^G(\boldsymbol{u}) = \int_{\mathcal{B}} (\psi^e(\boldsymbol{\varepsilon} - \boldsymbol{\varepsilon}^p) + \psi^p(\alpha))\,\mathrm{d}V + \Pi^{ext}(\boldsymbol{u}) \tag{4}$$

depending on the elastic free energy function ψ^e formulated in terms of the elastic strains $(3)_2$, i.e.

$$\psi^e(\boldsymbol{\varepsilon} - \boldsymbol{\varepsilon}^p) = \frac{1}{2}(\boldsymbol{\varepsilon} - \boldsymbol{\varepsilon}^p) : \mathbb{C} : (\boldsymbol{\varepsilon} - \boldsymbol{\varepsilon}^p)\,. \tag{5}$$

where $\mathbb{C}$ denotes the fourth-order elasticity tensor. The plastic part of the energy ψ^p is formulated in terms of the internal variable α, the external potential $\Pi^{ext}(\boldsymbol{u})$ is given by

$$\Pi^{ext}(\boldsymbol{u}) = -\int_{\mathcal{B}} \boldsymbol{f}\cdot\boldsymbol{u}\,\mathrm{d}V - \int_{\partial\mathcal{B}_t} \boldsymbol{t}\cdot\boldsymbol{u}\,\mathrm{d}A \tag{6}$$

with the body forces $\boldsymbol{f}$ and traction vector $\boldsymbol{t}$. Applying a Legendre transformation for the free energy function allows the introduction of the stress tensor $\boldsymbol{\sigma}$ as an additional independent variable

$$\psi^e(\boldsymbol{\varepsilon} - \boldsymbol{\varepsilon}^p) = \boldsymbol{\sigma} : (\boldsymbol{\varepsilon} - \boldsymbol{\varepsilon}^p) - \chi(\boldsymbol{\sigma})\,. \tag{7}$$

In the case of linear elasticity, we simply obtain

$$\chi(\boldsymbol{\sigma}) = \frac{1}{2}\boldsymbol{\sigma} : \mathbb{C}^{-1} : \boldsymbol{\sigma} \tag{8}$$

where $\chi(\boldsymbol{\sigma})$ denotes the complementary stored energy and the compliance tensor $\mathbb{C}^{-1}$ is defined as the inverse of the fourth-order elasticity tensor. In isotropic linear elasticity the compliance tensor is given as

$$\mathbb{C}^{-1} := \frac{1}{2\mu}\mathbb{I} - \frac{\Lambda}{2\mu(2\mu+3\Lambda)}\boldsymbol{1}\otimes\boldsymbol{1}\,, \tag{9}$$

with the second-order identity tensor $\mathbf{1}$, the dyadic product defined by $(\mathbf{1}\otimes\mathbf{1})_{ijkl}=\delta_{ij}\delta_{kl}$, the fourth-order identity tensor $\mathbb{I}_{ijkl}=\frac{1}{2}(\delta_{il}\delta_{jk}+\delta_{ik}\delta_{jl})$ and the Lamé constants Λ and μ. Substituting (7) into (4) yields the Prange-Hellinger-Reissner functional

$$\Pi^{PHR}(\boldsymbol{\sigma},\boldsymbol{u})=\int_{\mathcal{B}}(\boldsymbol{\sigma}:(\boldsymbol{\varepsilon}-\boldsymbol{\varepsilon}^p)-\chi(\boldsymbol{\sigma})+\psi^p(\alpha))\,\mathrm{d}V+\Pi^{ext}(\boldsymbol{u})\,, \tag{10}$$

depending on the stress and displacement fields. In order to find the stationary point of the functional, we have to calculate the roots of the first variations with respect to the unknown fields $\boldsymbol{u}$ and $\boldsymbol{\sigma}$. In detail, we obtain

$$\begin{aligned} G_u:=\delta_{\boldsymbol{u}}\Pi &= \int_{\mathcal{B}}\delta\boldsymbol{\varepsilon}:\boldsymbol{\sigma}\,\mathrm{d}V-\int_{\mathcal{B}}\delta\boldsymbol{u}\cdot\boldsymbol{f}\,\mathrm{d}V-\int_{\partial\mathcal{B}_t}\delta\boldsymbol{u}\cdot\boldsymbol{t}\,\mathrm{d}A\,,\\ G_\sigma:=\delta_{\boldsymbol{\sigma}}\Pi &= \int_{\mathcal{B}}(\delta\boldsymbol{\sigma}:(\boldsymbol{\varepsilon}-\boldsymbol{\varepsilon}^p)-\delta\boldsymbol{\sigma}:\partial_{\boldsymbol{\sigma}}\chi(\boldsymbol{\sigma}))\,\mathrm{d}V\,, \end{aligned} \tag{11}$$

with the virtual displacements $\delta\boldsymbol{u}$, the virtual stress field $\delta\boldsymbol{\sigma}$. Furthermore, the virtual strains are defined by

$$\delta\boldsymbol{\varepsilon}:=\nabla^s\delta\boldsymbol{u}=\frac{1}{2}(\nabla\delta\boldsymbol{u}+(\nabla\delta\boldsymbol{u})^T)\,. \tag{12}$$

The associated Euler-Lagrange equations, extracted from $G_u=0$ and $G_\sigma=0$, follow directly from a straight-forward reformulation of the weak forms

$$\begin{aligned} G_u &= -\int_{\mathcal{B}}\delta\boldsymbol{u}\cdot(\operatorname{div}\boldsymbol{\sigma}+\boldsymbol{f})\,\mathrm{d}V \qquad \rightarrow \quad \operatorname{div}\boldsymbol{\sigma}+\boldsymbol{f}=\mathbf{0}\,,\\ G_\sigma &= \int_{\mathcal{B}}\delta\boldsymbol{\sigma}:(\boldsymbol{\varepsilon}-\boldsymbol{\varepsilon}^p-\partial_{\boldsymbol{\sigma}}\chi(\boldsymbol{\sigma}))\,\mathrm{d}V \quad \rightarrow \quad \boldsymbol{\varepsilon}-\boldsymbol{\varepsilon}^p=\partial_{\boldsymbol{\sigma}}\chi(\boldsymbol{\sigma})\,. \end{aligned} \tag{13}$$

Obviously, the term $\partial_{\boldsymbol{\sigma}}\chi(\boldsymbol{\sigma})$ characterizes the elastic strains $\boldsymbol{\varepsilon}^e$. In order to guarantee the thermodynamical admissibility of the constitutive relations, we use the second law of thermodynamics by means of the Clausius-Duhem inequality. Inserting the material time derivative of the free energy function $\psi=\psi^e+\psi^p$ into $\mathcal{D}=\boldsymbol{\sigma}:\dot{\boldsymbol{\varepsilon}}-\dot{\psi}\geq 0$ yields

$$\mathcal{D} = \boldsymbol{\sigma}:\dot{\boldsymbol{\varepsilon}}-\{\dot{\boldsymbol{\sigma}}:(\boldsymbol{\varepsilon}-\boldsymbol{\varepsilon}^p)+\boldsymbol{\sigma}:(\dot{\boldsymbol{\varepsilon}}-\dot{\boldsymbol{\varepsilon}}^p)-\partial_{\boldsymbol{\sigma}}\chi:\dot{\boldsymbol{\sigma}}+\partial_\alpha\psi^p\,\dot{\alpha}\} \geq 0\,. \tag{14}$$

This holds for linear as well as for nonlinear hardening laws if $\partial_\alpha\phi>0$ ($h>0$). For reasons of simplicity we restrict ourselves to linear isotropic hardening. Thus, the hardening potential $\psi^p(\alpha)$ is given by

$$\psi^p(\alpha)=y_0\alpha+\frac{1}{2}h\alpha^2\,. \tag{15}$$

Inserting the abbreviation $\beta=-\partial_\alpha\psi^p$, the Clausius-Duhem inequality reads

$$\begin{aligned} \mathcal{D} &= \boldsymbol{\sigma}:\dot{\boldsymbol{\varepsilon}}^p+\dot{\boldsymbol{\sigma}}:(\partial_{\boldsymbol{\sigma}}\chi-(\boldsymbol{\varepsilon}-\boldsymbol{\varepsilon}^p))+\beta\dot{\alpha} \geq 0\\ &= \boldsymbol{\sigma}:\dot{\boldsymbol{\varepsilon}}^p+\dot{\boldsymbol{\sigma}}:(\partial_{\boldsymbol{\sigma}}\chi-\boldsymbol{\varepsilon}^e)+\beta\dot{\alpha} \geq 0\,. \end{aligned} \tag{16}$$

Substituting the Euler-Lagrange equation $(13)_2$, we obtain the reduced dissipation inequality

$$\mathcal{D}^{int}=\boldsymbol{\sigma}:\dot{\boldsymbol{\varepsilon}}^p+\beta\dot{\alpha}\geq 0\,. \tag{17}$$

For the framework of elasto-plasticity, we determine the internal variables by means of the principle of maximum plastic dissipation, i.e. we identify from all possible states, which satisfy the yield criterion, the one that maximizes plastic dissipation. This implies an associated flow rule, the loading/unloading conditions in Kuhn-Tucker form and convexity of the elastic range, compare e.g. Simo [1988a;b] and Simo and Hughes [1998]. With this in hand, we construct a Lagrangian functional $\mathcal{L}$

$$\mathcal{L}(\boldsymbol{\sigma}, \beta, \lambda) = -\mathcal{D}^{int} + \lambda \Phi(\boldsymbol{\sigma}, \beta) \tag{18}$$

with the von Mises yield criterion

$$\Phi(\boldsymbol{\sigma}, \beta) = ||\operatorname{dev} \boldsymbol{\sigma}|| + \sqrt{\frac{2}{3}}\beta \leq 0 \tag{19}$$

and the plastic multiplier $\lambda \geq 0$. The principle of maximum plastic dissipation postulates an extreme value for the Lagrangian functional, i.e. $\mathcal{L}(\boldsymbol{\sigma}, \beta, \lambda) \rightarrow$ stat., in addition with the loading/unloading conditions

$$\lambda \geq 0, \quad \Phi \leq 0 \quad \text{and} \quad \lambda\Phi = 0\,. \tag{20}$$

Enforcing stationarity of the functional by building the first derivative with respect to all unknowns yields the evolution of the internal variables and the consistency condition, i.e.

$$\begin{aligned} \partial_{\boldsymbol{\sigma}}\mathcal{L} &= -\dot{\boldsymbol{\varepsilon}}^p + \lambda \partial_{\boldsymbol{\sigma}} \Phi(\boldsymbol{\sigma}, \beta) &&= 0\,, \\ \partial_{\beta}\mathcal{L} &= -\dot{\alpha} + \lambda \partial_{\beta} \Phi(\boldsymbol{\sigma}, \beta) &&= 0\,, \\ \partial_{\lambda}\mathcal{L} &= \Phi(\boldsymbol{\sigma}, \beta) &&= 0\,. \end{aligned} \tag{21}$$

The rate equation for the plastic strains and the internal variable then yields

$$\begin{aligned} \dot{\boldsymbol{\varepsilon}}^p &= \lambda \partial_{\boldsymbol{\sigma}} \Phi(\boldsymbol{\sigma}, \beta) = \lambda \frac{\operatorname{dev} \boldsymbol{\sigma}}{||\operatorname{dev} \boldsymbol{\sigma}||} = \lambda \boldsymbol{n}\,, \\ \dot{\alpha} &= \lambda \partial_{\beta} \Phi(\boldsymbol{\sigma}, \beta) = \lambda \sqrt{\frac{2}{3}}\,. \end{aligned} \tag{22}$$

Applying a backward Euler integration scheme on the time interval $[t_n, t_{n+1}]$, the discrete internal variables at time t_{n+1} are

$$\boldsymbol{\varepsilon}^p_{n+1} = \boldsymbol{\varepsilon}^p_n + \underbrace{\gamma\, \boldsymbol{n}_{n+1}}_{\Delta_t \boldsymbol{\varepsilon}^p_{n+1}} \quad \text{and} \quad \alpha_{n+1} = \alpha_n + \underbrace{\sqrt{\frac{2}{3}}\gamma}_{\Delta_t \alpha_{n+1}}\,, \tag{23}$$

where we have used the abbreviation $\gamma := \lambda\, \Delta t$ with $\Delta t = t_{n+1} - t_n$. In order to avoid confusion in the forthcoming linearization procedure, we denote the increment of the plastic strains with $\Delta_t \boldsymbol{\varepsilon}^p_{n+1}$ and $\Delta_t \alpha_{n+1}$ for the internal variable. For applying the Newton method, we need the linearization of the discrete counterpart of (11) at time t_{n+1}. For the computation of the plastic multiplier, we have to enforce

$$\Phi(\boldsymbol{\sigma}_{n+1}, \beta_{n+1}) = ||\operatorname{dev} \boldsymbol{\sigma}_{n+1}|| + \sqrt{\frac{2}{3}}\beta_{n+1} \stackrel{!}{=} 0\,, \tag{24}$$

and define based on $\beta_n = \beta^{trial}$ a trial state of the yield function Φ^{trial} as

$$\Phi^{trial} := \Phi(\boldsymbol{\sigma}_{n+1}, \beta_n) = ||\operatorname{dev} \boldsymbol{\sigma}_{n+1}|| + \sqrt{\frac{2}{3}}\beta_n \tag{25}$$

with $\beta_n = -(y_0 + h\alpha_n)$. The state of plasticity within the formulation is distinguished into in an elastic/neutral and a plastic loading, which is determined by means of the yield function. Taking into account the trial state of the yield function (25), we obtain for elastic/neutral loading if

$$\Phi^{trial} \leq 0\,, \tag{26}$$

and plastic loading if

$$\Phi^{trial} > 0\,. \tag{27}$$

Taking into account condition (24) and $(23)_2$ as well as $\beta_{n+1} = \beta_n - h\Delta_t\alpha_{n+1} = \beta_n - h\sqrt{\frac{2}{3}}\gamma$ we compute the discrete plastic multiplier

$$\gamma = \frac{3\Phi^{trial}}{2h}\,. \tag{28}$$

Substituting this quantity into (23) yields the plastic strains and hardening parameter at time t_{n+1}, see e.g. Simo and Hughes [1998]. The associated first variations appear as

$$\begin{aligned} G_u^{n+1} &= \int_{\mathcal{B}} \delta\boldsymbol{\varepsilon} : \boldsymbol{\sigma}_{n+1}\,\mathrm{d}V - \int_{\mathcal{B}} \delta\boldsymbol{u}\cdot\boldsymbol{f}_{n+1}\,\mathrm{d}V - \int_{\partial\mathcal{B}_t} \delta\boldsymbol{u}\cdot\boldsymbol{t}_{n+1}\,\mathrm{d}A\,, \\ G_\sigma^{n+1} &= \int_{\mathcal{B}} \delta\boldsymbol{\sigma} : (\boldsymbol{\varepsilon}_{n+1} - \boldsymbol{\varepsilon}^p_{n+1} - \partial_{\boldsymbol{\sigma}}\chi(\boldsymbol{\sigma}_{n+1}))\,\mathrm{d}V\,, \end{aligned} \tag{29}$$

with $\partial_{\boldsymbol{\sigma}}\chi(\boldsymbol{\sigma}_{n+1}) =: \boldsymbol{\varepsilon}^e_{n+1}(\boldsymbol{\sigma}_{n+1}) = \mathbb{C}^{-1} : \boldsymbol{\sigma}_{n+1}$. The linearization yields

$$\begin{aligned} \Delta G_u^{n+1} &= \int_{\mathcal{B}} \delta\boldsymbol{\varepsilon} : \Delta\boldsymbol{\sigma}_{n+1}\,\mathrm{d}V\,, \\ \Delta G_\sigma^{n+1} &= \int_{\mathcal{B}} \delta\boldsymbol{\sigma} : (\Delta\boldsymbol{\varepsilon}_{n+1} - \Delta\{\boldsymbol{\varepsilon}^p_{n+1}\} - \partial^2_{\boldsymbol{\sigma}\boldsymbol{\sigma}}\chi(\boldsymbol{\sigma}_{n+1}) : \Delta\boldsymbol{\sigma}_{n+1})\,\mathrm{d}V\,, \end{aligned} \tag{30}$$

with $\partial^2_{\boldsymbol{\sigma}\boldsymbol{\sigma}}\chi(\boldsymbol{\sigma}_{n+1}) : \Delta\boldsymbol{\sigma}_{n+1} = \mathbb{C}^{-1} : \Delta\boldsymbol{\sigma}_{n+1} = \Delta\boldsymbol{\varepsilon}^e_{n+1}(\boldsymbol{\sigma}_{n+1})$. The term $\Delta\{\boldsymbol{\varepsilon}^p_{n+1}\}$ denotes the linearization of the plastic strains $\boldsymbol{\varepsilon}^p_{n+1}$ with respect to the stresses, i.e.

$$\Delta\{\boldsymbol{\varepsilon}^p_{n+1}\} = \Delta\{\boldsymbol{\varepsilon}^p_n + \Delta_t\boldsymbol{\varepsilon}^p_{n+1}\} = \Delta\gamma\,\boldsymbol{n}_{n+1} + \gamma\,\Delta\boldsymbol{n}_{n+1}\,. \tag{31}$$

Determining the linearization of the plastic strains by applying the chain rule, we obtain for the linear increment of the plastic multiplier

$$\Delta\gamma = \frac{3\Delta\Phi^{trial}}{2h} = \frac{3}{2h}\boldsymbol{n}_{n+1} : \Delta\boldsymbol{\sigma}_{n+1}\,. \tag{32}$$

The linearization of the outward normal on the deviatoric stress plane yields

$$\Delta\boldsymbol{n}_{n+1} = -\frac{1}{||\operatorname{dev}\boldsymbol{\sigma}_{n+1}||}(\boldsymbol{n}_{n+1}\otimes\boldsymbol{n}_{n+1} - \mathbb{P}) : \Delta\boldsymbol{\sigma}_{n+1} \tag{33}$$

where the fourth-order deviatoric projection tensor is given by $\mathbb{P} = \mathbb{I} - \frac{1}{3}\mathbf{1}\otimes\mathbf{1}$. Thus, we receive with

$$\Delta\{\boldsymbol{\varepsilon}^p_{n+1}\} = \underbrace{\left(\left(\frac{3}{2\,h} - \frac{\gamma}{||\operatorname{dev}\boldsymbol{\sigma}_{n+1}||}\right)\boldsymbol{n}_{n+1}\otimes\boldsymbol{n}_{n+1} + \frac{\gamma}{||\operatorname{dev}\boldsymbol{\sigma}_{n+1}||}\mathbb{P}\right)}_{:=\boldsymbol{\Xi}_{n+1}} : \Delta\boldsymbol{\sigma}_{n+1}\,, \tag{34}$$

see e.g. Schröder et al. [1997], the expression for the linearization of $(30)_2$ as

$$\Delta G^{n+1}_\sigma = \int_{\mathcal{B}} \delta\boldsymbol{\sigma} : \{\Delta\boldsymbol{\varepsilon}_{n+1} - \boldsymbol{\Xi}_{n+1} : \Delta\boldsymbol{\sigma}_{n+1} - \partial^2_{\boldsymbol{\sigma}\boldsymbol{\sigma}}\chi(\boldsymbol{\sigma}_{n+1}) : \Delta\boldsymbol{\sigma}_{n+1}\}\,\mathrm{d}V\,, \tag{35}$$

and finally

$$\Delta G^{n+1}_\sigma = \int_{\mathcal{B}} \delta\boldsymbol{\sigma} : \{\Delta\boldsymbol{\varepsilon}_{n+1} - \mathbb{D}^{ep}_{n+1} : \Delta\boldsymbol{\sigma}_{n+1}\}\,\mathrm{d}V\,, \tag{36}$$

where

$$\mathbb{D}^{ep}_{n+1} := \boldsymbol{\Xi}_{n+1} + \partial^2_{\boldsymbol{\sigma}\boldsymbol{\sigma}}\chi(\boldsymbol{\sigma}_{n+1}) = \boldsymbol{\Xi}_{n+1} + \mathbb{C}^{-1} \tag{37}$$

denotes the algorithmic consistent fourth-order *inverse* material tangent for elasto-plasticity.

2.1 Discretization

In this subsection, we consider the discretized problem by inserting the interpolation of the stresses, displacements and related fields (see also Appendix A). In the following underlined values $(\underline{\bullet})$ denotes the matrix notation of the value $(\bullet)$; i.e.

$$\left.\begin{array}{rclrclrcl}
\underline{\boldsymbol{\sigma}}_{n+1} &=& \underline{\boldsymbol{S}}\boldsymbol{\beta}_{n+1}\,, & \underline{\boldsymbol{u}}_{n+1} &=& \underline{\boldsymbol{N}}\boldsymbol{d}_{n+1}\,, & \underline{\boldsymbol{\varepsilon}}_{n+1} &=& \underline{\boldsymbol{B}}\boldsymbol{d}_{n+1} \\
\delta\underline{\boldsymbol{\sigma}}_{n+1} &=& \underline{\boldsymbol{S}}\delta\boldsymbol{\beta}_{n+1}\,, & \delta\underline{\boldsymbol{u}}_{n+1} &=& \underline{\boldsymbol{N}}\delta\boldsymbol{d}_{n+1}\,, & \delta\underline{\boldsymbol{\varepsilon}}_{n+1} &=& \underline{\boldsymbol{B}}\delta\boldsymbol{d}_{n+1} \\
\Delta\underline{\boldsymbol{\sigma}}_{n+1} &=& \underline{\boldsymbol{S}}\Delta\boldsymbol{\beta}_{n+1}\,, & \Delta\underline{\boldsymbol{u}}_{n+1} &=& \underline{\boldsymbol{N}}\Delta\boldsymbol{d}_{n+1}\,, & \Delta\underline{\boldsymbol{\varepsilon}}_{n+1} &=& \underline{\boldsymbol{B}}\Delta\boldsymbol{d}_{n+1}
\end{array}\right\}. \tag{38}$$

For convenience the index $n+1$ for the obvious terms is omitted in the following. The discretized weak forms $G^h_u = \sum_e G^e_u$ and $G^h_\sigma = \sum_e G^e_\sigma$ for a typical element $\mathcal{B}^e$ appear as

$$\begin{aligned}
G^e_u &= \delta\boldsymbol{d}^T \int_{\mathcal{B}^e} \underline{\boldsymbol{B}}^T\underline{\boldsymbol{\sigma}}\,\mathrm{d}V - \delta\boldsymbol{d}^T \int_{\mathcal{B}^e} \underline{\boldsymbol{N}}^T\boldsymbol{f}\,\mathrm{d}V - \delta\boldsymbol{d}^T \int_{\partial\mathcal{B}^e_t} \underline{\boldsymbol{N}}^T\boldsymbol{t}\,\mathrm{d}A\,, \\
G^e_\sigma &= \delta\boldsymbol{\beta}^T \int_{\mathcal{B}^e} \underline{\boldsymbol{S}}^T(\underline{\boldsymbol{\varepsilon}} - \underline{\boldsymbol{\varepsilon}}^p - \partial_{\boldsymbol{\sigma}}\chi(\underline{\boldsymbol{\sigma}}))\,\mathrm{d}V\,.
\end{aligned} \tag{39}$$

The linearization of the weak forms, $\mathrm{Lin}G^e_{u,\sigma} = G^e_{u,\sigma}(\boldsymbol{d},\boldsymbol{\beta}) + \Delta G^e_{u,\sigma}(\Delta\boldsymbol{d},\Delta\boldsymbol{\beta})$, yields the increments

$$\begin{aligned}
\Delta G^e_u &= \delta\boldsymbol{d}^T \int_{\mathcal{B}^e} \underline{\boldsymbol{B}}^T\underline{\boldsymbol{S}}\,\mathrm{d}V\Delta\boldsymbol{\beta}\,, \\
\Delta G^e_\sigma &= \delta\boldsymbol{\beta}^T \int_{\mathcal{B}^e} \underline{\boldsymbol{S}}^T\underline{\boldsymbol{B}}\,\mathrm{d}V\Delta\boldsymbol{d} - \delta\boldsymbol{\beta}^T \int_{\mathcal{B}^e} \underline{\boldsymbol{S}}^T\mathbb{D}^{ep}\underline{\boldsymbol{S}}\,\mathrm{d}V\Delta\boldsymbol{\beta}\,.
\end{aligned} \tag{40}$$

For the last reformulation of the system, we introduce for convenience the element matrices

$$\underline{\boldsymbol{G}}^e := \int_{\mathcal{B}^e} \underline{\boldsymbol{S}}^T \underline{\boldsymbol{B}} \, \mathrm{d}V \quad \text{and} \quad \underline{\boldsymbol{H}}^e := \int_{\mathcal{B}^e} \underline{\boldsymbol{S}}^T \underline{\mathbb{D}}^{ep} \underline{\boldsymbol{S}} \, \mathrm{d}V \,. \tag{41}$$

The right hand side vector for a typical element regarding the displacements is

$$\underline{\boldsymbol{r}}_u^e := \int_{\mathcal{B}^e} \underline{\boldsymbol{B}}^T \boldsymbol{\sigma} \, \mathrm{d}V - \int_{\mathcal{B}^e} \underline{\boldsymbol{N}}^T \boldsymbol{f} \, \mathrm{d}V - \int_{\partial \mathcal{B}_t^e} \underline{\boldsymbol{N}}^T \boldsymbol{t} \, \mathrm{d}A \,, \tag{42}$$

and for the term related to the stresses we obtain

$$\underline{\boldsymbol{r}}_\sigma^e := \int_{\mathcal{B}^e} \underline{\boldsymbol{S}}^T (\underline{\boldsymbol{\varepsilon}} - \underline{\boldsymbol{\varepsilon}}^p - \partial_{\boldsymbol{\sigma}} \chi(\underline{\boldsymbol{\sigma}})) \, \mathrm{d}V \,. \tag{43}$$

Inserting $\underline{\boldsymbol{G}}^e$ and $\underline{\boldsymbol{H}}^e$ yields the system of equations as

$$\begin{aligned} \mathrm{Lin} G_u^e &= \delta \boldsymbol{d}^T (\underline{\boldsymbol{r}}_u^e + \underline{\boldsymbol{G}}^{eT} \Delta \boldsymbol{\beta}) \,, \\ \mathrm{Lin} G_\sigma^e &= \delta \boldsymbol{\beta}^T (\underline{\boldsymbol{r}}_\sigma^e + \underline{\boldsymbol{G}}^e \Delta \boldsymbol{d} - \underline{\boldsymbol{H}}^e \Delta \boldsymbol{\beta}) \,. \end{aligned} \tag{44}$$

The discontinuous stress approximation allows (if the inverse of $\underline{\boldsymbol{H}}^e$ exists) a static condensation of the stresses. We obtain, by solving $\mathrm{Lin} G_\sigma^e = 0$,

$$\Delta \boldsymbol{\beta} = \underline{\boldsymbol{H}}^{e-1} \underline{\boldsymbol{r}}_\sigma^e + \underline{\boldsymbol{H}}^{e-1} \underline{\boldsymbol{G}}^e \Delta \boldsymbol{d} = \bar{\underline{\boldsymbol{r}}}_\sigma + \bar{\underline{\boldsymbol{k}}}_\sigma \Delta \boldsymbol{d} \,. \tag{45}$$

Substituting the expression for the stress degree of freedom into $(44)_1$ yields the condensed system depending only on the incremental displacements

$$\mathrm{Lin} G_u^e = \delta \boldsymbol{d}^T (\underbrace{\underline{\boldsymbol{r}}_u^e + \underline{\boldsymbol{G}}^{eT} \underline{\boldsymbol{H}}^{e-1} \underline{\boldsymbol{r}}_\sigma^e}_{\underline{\boldsymbol{r}}^e} + \underbrace{\underline{\boldsymbol{G}}^{eT} \underline{\boldsymbol{H}}^{e-1} \underline{\boldsymbol{G}}^e}_{\underline{\boldsymbol{k}}^e} \Delta \boldsymbol{d}) \,. \tag{46}$$

Assembling over the number of finite elements (num_{ele}) leads to the global system of equations

$$\mathop{\mathsf{A}}_{e=1}^{num_{ele}} \delta \boldsymbol{d}^T (\underline{\boldsymbol{r}}^e + \underline{\boldsymbol{k}}^e \Delta \boldsymbol{d}) = \delta \boldsymbol{D} (\boldsymbol{R} + \boldsymbol{K} \Delta \boldsymbol{D}) = 0 \tag{47}$$

and therefore the nodal displacement are computed via

$$\Delta \boldsymbol{D} = -\boldsymbol{K}^{-1} \boldsymbol{R} \,. \tag{48}$$

The related algorithmic treatment for the implementation of the derived formulation for elasto-plasticity at small strains under plane stress conditions are summarized in Table 1.

2.2 Enforcement of plane strain condition

Additionally, for considering the framework of plane strain elasto-plasticity within the mixed Prange-Hellinger-Reissner element formulation, we deduce a local plane strain algorithm in analogy to the publications of De Borst [1991] and Klinkel and Govindjee

Variables without any indices are given at iteration k+1 and time t_{n+1}

(1) Update of the displacements (Newton iteration k+1)

Read from history $\underline{\boldsymbol{\varepsilon}}_n^p, \sigma_{33n}, \alpha_n, \boldsymbol{\beta}_n^{(k)}, \bar{\underline{\boldsymbol{r}}}_\sigma^{(k)}$ and $\bar{\underline{\boldsymbol{k}}}_\sigma^{(k)}$

$\boldsymbol{d} = \boldsymbol{d}_n^{(k)} + \Delta\boldsymbol{d}$ and $\boldsymbol{\beta} = \boldsymbol{\beta}_n^{(k)} + \Delta\boldsymbol{\beta}$ with $\Delta\boldsymbol{\beta} = \bar{\boldsymbol{r}}_\sigma^{(k)} + \bar{\boldsymbol{k}}_\sigma^{(k)}\Delta\boldsymbol{d}$

GAUSS LOOP (2) - (4)

(2) Compute stresses at each Gauss Point with $\underline{\boldsymbol{\sigma}} = \underline{\boldsymbol{S}}\boldsymbol{\beta}$

(3) IF plane stress condition THEN

$\Phi^{trial} = ||\operatorname{dev}\boldsymbol{\sigma}_{n+1}|| - \sqrt{\frac{2}{3}}\beta_n$

IF $\Phi^{trial} \leq 0$ THEN

$\boldsymbol{\varepsilon}^p = \boldsymbol{\varepsilon}_n^p$ and $\alpha = \alpha_n$

ELSE IF $\Phi^{trial} > 0$:

$\gamma = \frac{3\Phi^{trial}}{2h}, \boldsymbol{\varepsilon}^p = \boldsymbol{\varepsilon}_n^p + \gamma\boldsymbol{n}$ and $\alpha = \alpha_n + \sqrt{\frac{2}{3}}\gamma$

ELSE IF plane strain condition THEN GO TO Table 2

END IF

(4) Determine element matrices and vectors

$$\underline{\boldsymbol{H}}^e = \int_{\mathcal{B}^e} \underline{\boldsymbol{S}}^T \underline{\mathbb{D}}^{ep} \underline{\boldsymbol{S}}\, \mathrm{d}V \text{ and } \underline{\boldsymbol{G}}^e = \int_{\mathcal{B}^e} \underline{\boldsymbol{S}}^T \underline{\boldsymbol{B}}\, \mathrm{d}V$$

$$\underline{\boldsymbol{r}}_\sigma^e = \int_{\mathcal{B}^e} \underline{\boldsymbol{S}}^T (\underline{\boldsymbol{\varepsilon}} - \underline{\boldsymbol{\varepsilon}}^p - \underline{\boldsymbol{\varepsilon}}^e)\, \mathrm{d}V$$

(5) Calculate vector and matrix for local stress computation

$\bar{\underline{\boldsymbol{r}}}_\sigma := \underline{\boldsymbol{H}}^{e-1}\underline{\boldsymbol{r}}_\sigma^e$ and $\bar{\underline{\boldsymbol{k}}}_\sigma := \underline{\boldsymbol{H}}^{e-1}\underline{\boldsymbol{G}}^e$

(6) Determine right hand side vector and element stiffness matrix

$\underline{\boldsymbol{r}}^e := \underline{\boldsymbol{G}}^{eT}(\boldsymbol{\beta} + \bar{\underline{\boldsymbol{r}}}_\sigma)$ and $\underline{\boldsymbol{k}}^e := \underline{\boldsymbol{G}}^{eT}\bar{\underline{\boldsymbol{k}}}_\sigma$

(7) Write in history $\underline{\boldsymbol{\varepsilon}}^p, \alpha, \sigma_{33}, \boldsymbol{\beta}, \bar{\underline{\boldsymbol{r}}}_\sigma$ and $\bar{\underline{\boldsymbol{k}}}_\sigma$

(8) Assembling, see equation (47), and solving the system of equations (48)

Table 1: Algorithmic treatment for the elasto-plastic mixed formulation

[2002]. The requirement of plane strain conditions are given by $\varepsilon_{13} = \varepsilon_{23} = \varepsilon_{33} = 0$ resulting, in general, in a non-zero σ_{33}. For enforcing the zero-strain condition, we regard a vector representation of the incremental elasto-plastic constitutive equation, which reads

$$\Delta\underline{\boldsymbol{\varepsilon}} = \underline{\mathbb{D}}^{ep}\Delta\underline{\boldsymbol{\sigma}} \quad \Rightarrow \quad \begin{pmatrix} \Delta\boldsymbol{\varepsilon}_m \\ \Delta\varepsilon_z \end{pmatrix} = \begin{pmatrix} \mathbb{D}_{mm}^{ep} & \mathbb{D}_{mz}^{ep} \\ \mathbb{D}_{zm}^{ep} & \mathbb{D}_{zz}^{ep} \end{pmatrix} \begin{pmatrix} \Delta\boldsymbol{\sigma}_m \\ \Delta\sigma_z \end{pmatrix}, \tag{49}$$

where $\mathbb{D}^{ep}_{mm} \in \mathbb{R}^{3\times3}$, $\mathbb{D}^{ep}_{mz} \in \mathbb{R}^{3\times1}$ and $\mathbb{D}^{ep}_{zm} \in \mathbb{R}^{1\times3}$ matrix. Further, $\mathbb{D}^{ep}_{zz}$ is given as a scalar value. Additionally, $\boldsymbol{\varepsilon}_m$ and ε_z are defined as

$$\boldsymbol{\varepsilon}_m = (\varepsilon_{11}, \varepsilon_{22}, 2\varepsilon_{12})^T \quad \text{and} \quad \varepsilon_z = (\varepsilon_{33}) = 0\,, \tag{50}$$

and $\boldsymbol{\sigma}_m$ and σ_z as

$$\boldsymbol{\sigma}_m = (\sigma_{11}, \sigma_{22}, \sigma_{12})^T \quad \text{and} \quad \sigma_z = (\sigma_{33})\,. \tag{51}$$

For the development of a local plane strain algorithm, we start from the vector representation (49). Regarding the plane strain condition we postulate that ε_z has to be zero enforced by the corresponding stress σ_z. The strain $\varepsilon_z^{(i+1)} = \varepsilon_z^{(i)} + \Delta\varepsilon_z$ can be expressed, using (49), as

$$\varepsilon_z^{(i+1)} = \varepsilon_z^{(i)} + \mathbb{D}^{ep}_{zz}\Delta\sigma_z \stackrel{!}{=} 0\,. \tag{52}$$

The update scheme for the stresses in the next local iteration step is given by

$$\Delta\sigma_z = -\mathbb{D}^{ep\,-1}_{zz}\varepsilon_z \quad \Rightarrow \quad \sigma_z^{(i+1)} = \sigma_z^{(i)} + \Delta\sigma_z\,. \tag{53}$$

In order to achieve quadratic convergence a modification of the elasto-plastic tangent modulus for the Newton iteration is necessary. Regarding the reduction of the strain and stress tensor to $\boldsymbol{\varepsilon}_m$ and $\boldsymbol{\sigma}_m$ the material tangent is still depending on the full stress state $\underline{\boldsymbol{\sigma}}$. Therefore, the overall material tangent has to be condensed due to the plane strain condition. A reformulation of $(49)_2$, exploiting $\Delta\varepsilon_z = \mathbb{D}^{ep}_{zm}\Delta\boldsymbol{\sigma}_m + \mathbb{D}^{ep}_{zz}\Delta\sigma_z$ with $\Delta\varepsilon_z = 0$ yields

$$\Delta\sigma_z = -\mathbb{D}^{ep\,-1}_{zz}\mathbb{D}^{ep}_{zm}\Delta\boldsymbol{\sigma}_m\,. \tag{54}$$

Substituting the latter expression into $(49)_1$ with $\Delta\boldsymbol{\varepsilon}_m = \mathbb{D}^{ep}_{mm}\Delta\boldsymbol{\sigma}_m + \mathbb{D}^{ep}_{mz}\Delta\sigma_z$ leads to the modified overall elasto-plastic material tangent $\mathbb{D}^{ep}_{mod}$ for plane strain condition,

$$\Delta\boldsymbol{\varepsilon}_m = \mathbb{D}^{ep}_{mod}\Delta\boldsymbol{\sigma}_m \quad \text{with} \quad \mathbb{D}^{ep}_{mod} = [\mathbb{D}^{ep}_{mm} - \mathbb{D}^{ep}_{mz}\mathbb{D}^{ep\,-1}_{zz}\mathbb{D}^{ep}_{zm}]\,. \tag{55}$$

(1) Read from history $\sigma_{33} = \sigma_{33n}$

Initialize $tol = 10^{-8}$

(2) Compute elastic and plastic strains

$$\boldsymbol{\sigma} = \begin{bmatrix} \sigma_{11} & \sigma_{12} & 0 \\ \sigma_{21} & \sigma_{22} & 0 \\ 0 & 0 & \sigma_{33} \end{bmatrix} \text{ with } \sigma_{21} = \sigma_{12}$$

$\boldsymbol{\varepsilon}^e = \mathbb{C}^{-1}\boldsymbol{\sigma}$

IF $\Phi^{trial} \leq 0$ THEN

$\boldsymbol{\varepsilon}^p = \boldsymbol{\varepsilon}^p_n$ and $\alpha = \alpha_n$

ELSE IF $\Phi^{trial} > 0$ THEN

$\gamma = \frac{3\Phi^{trial}}{2h}, \boldsymbol{\varepsilon}^p = \boldsymbol{\varepsilon}^p_n + \gamma \boldsymbol{n}$ and $\alpha = \alpha_n + \sqrt{\frac{2}{3}}\gamma$

END IF

$\varepsilon_{33} = \varepsilon^e_{33} + \varepsilon^p_{33}$

(3) Algorithmic consistent tangent

$$\mathbb{D}^{ep} = \mathbb{C}^{-1} + \partial_{\boldsymbol{\sigma}}\boldsymbol{\varepsilon}^p = \mathbb{C}^{-1} + \left(\frac{3}{2\,h} - \frac{\gamma}{||\operatorname{dev}\boldsymbol{\sigma}_{n+1}||}\right)\boldsymbol{n}_{n+1} \otimes \boldsymbol{n}_{n+1} + \frac{\gamma}{||\operatorname{dev}\boldsymbol{\sigma}_{n+1}||}\mathbb{P}$$

(4) Check for plane strain condition:

IF $|\varepsilon_{33}| < tol$ THEN GO TO (5)

$\sigma_{33} = \sigma_{33} + \Delta\sigma_{33}$ with $\Delta\sigma_{33} = \varepsilon_{33}/\mathbb{D}^{ep}_{3333}$ THEN GO TO (2)

(5) Plane strain modification for material tangent $\mathbb{D}^{ep}$

$\mathbb{D}^{ep}_{mod} = \mathbb{D}^{ep}_{mm} - \mathbb{D}^{ep}_{mz}\mathbb{D}^{ep\,-1}_{zz}\mathbb{D}^{ep}_{zm}$

Write in history σ_{33} and continue with Table 1

Table 2: Algorithm for the local enforcement of plane strain condition

3. Numerical simulations

In the following different types of boundary value problems are presented. Therefore, we first compare the standard displacement formulation, the proposed element formulation with a point-wise enforcement of the flow rule and the formulation presented in Simo et al. [1989] with an element-wise enforcement of the flow rule. The calculations are performed based on the assumption of plane stress conditions. The numerical examples considered here with the Cook's membrane problem and the extension of a perforated plate are given in Simo et al. [1989] where we choose for both examples a thickness of 1 {length}. Additionally, the results for the proposed formulation are compared with the one obtained by Simo et al. [1989] due to performance and accuracy. In this academic examples the units are defined in {force} and {length}, see Simo et al. [1989]. The examples should present the possibility and comparability to enforce the flow rule point-wise instead of an element-wise enforcement.
A second aspect which is the performance of the proposed element formulation under the assumption of plane strain conditions is shown on the example of an elongation of a plate with circular inclusion. For a better overview different fields e.g. stresses and plastic strains are shown in comparison with other well-known methods. Here, given as the standard displacement element (Q1) and the mixed Q1P0 element with an additional constant pressure field over the element domain.

3.1. Bending of Cook's membrane problem

The following example, Cook's membrane problem, see Cook [1974], is taken from Simo et al. [1989]. Here, the material and geometrical setup is depicted in Figure 1. The force F is applied on the right edge of the Cook's membrane acting in x_2-direction. Furthermore, we assume plane stress conditions. We compare the proposed mixed Prange-Hellinger-Reissner formulation with a Galerkin displacement formulation (Q1, bilinear quadrilateral element) and a mixed Galerkin formulation given by the Q1P0 element (Q1 element with an additional constant pressure field). A convergence study for the u_2 displacement of the top, right corner node (48,60) is shown in Figure 2. The PHR formulation with an element-wise enforcement of the flow rule, taken from Simo et al. [1989], is also depicted.

Setup of BVP

Left edge	$u_1 = u_2 = 0$
Right edge	$F = 1.8\,\{\text{force}\}$
Young's modulus	$E = 70\,\{\text{force}\}/\{\text{length}\}^2$
Poisson's ratio	$\nu = 0.3333$
Yield stress	$y_0 = 0.243\,\{\text{force}\}/\{\text{length}\}^2$
Hardening modulus	$h = 0.2\,\{\text{force}\}/\{\text{length}\}^2$

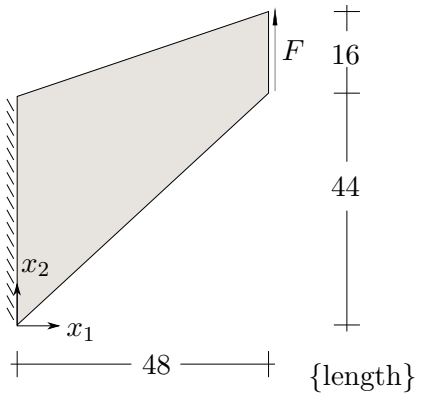

Figure 1: Geometrical and material setup for Cook's membrane problem

Regarding the computed results, all three formulations show a satisfactory convergence behavior. The solution for the mixed PHR formulation for a 64 element mesh is almost the same as for the mixed method with 256 Q1P0 elements or the displacement method

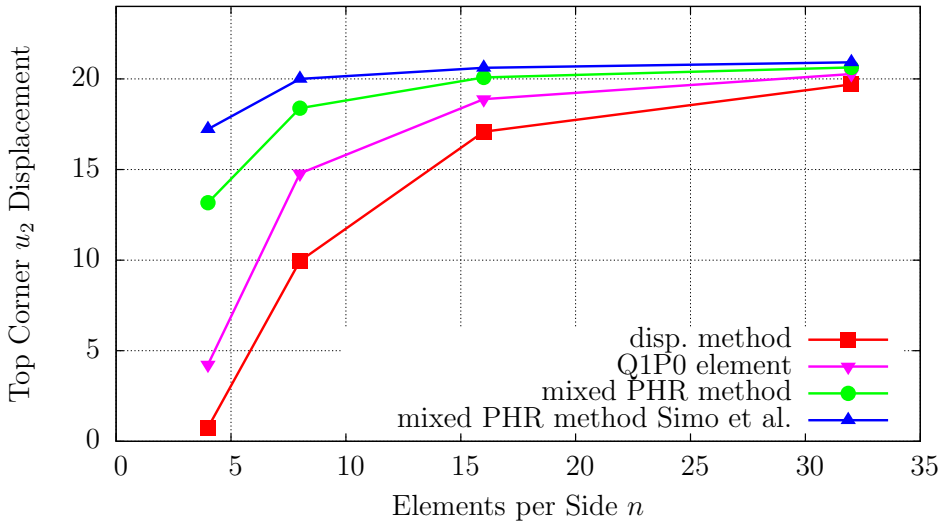

Figure 2: Convergence study for u_2 displacement of the top, right corner node (48,60) for Q1, Q1P0, mixed PHR formulation with point-wise and mixed PHR formulation with element-wise enforcement of the flow rule taken from Simo et al. [1989]

with 1024 Q1 elements. Thus, the mixed PHR element shows a much better efficiency and accuracy. The main goal of this contribution is to show the possibility of a point-wise enforcement of the flow rule which is shown within the convergence of the element formulation. A possible explanation for the better performance of the element formulation by Simo et al. [1989] could be given due to the additional iteration of the plastic multiplier over the element domain for performing a weak enforcement. Figure 3 shows the good agreement of the equivalent plastic strains for the different element formulations Q1, Q1P0 and PHR.

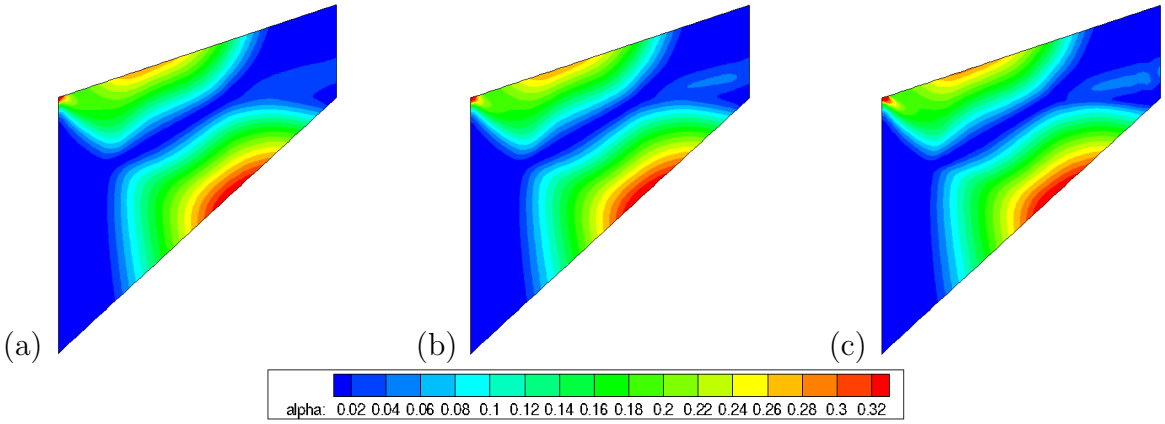

Figure 3: Distribution of equivalent plastic strains α for (a) the Q1, (b) the Q1P0 and (c) the presented PHR element formulation on the undeformed $n = 64$ element mesh under plane stress conditions for $F = 1.8$

The authors point out that the global effort for all three depicted element formulations are similar. In the proposed PHR formulation, we locally have a small increase in the effort due to the computation of the inverse matrix, which is however insignificant.
We can not confirm the statement by Simo et al. [1989] in Remark 2.1(2). Remark 2.1(2)

claims that a point-wise enforcement of the flow rule, hardening law and consistency condition recovers the displacement model. In the work of Simo et al. [1989] the hardening law and consistency condition are enforced point-wise whereas the flow rule is fulfilled in a weak sense over the element domain.
However, in the proposed formulation we enforce the flow rule, hardening law and consistency condition point-wise. As shown for example in Figure 2 the results of the proposed formulation do not coincide with the displacement model. Therefore, we can not confirm the statement of Simo et al. [1989] in Remark 2.1(2) in general. This is based on the fact that we still have a two field formulation with independent interpolations of the stresses and displacements and therefore do not recover the pure displacement formulation.

3.2. Extension of a perforated plate

As a second example, a perforated plate problem is investigated under plane stress assumptions, see Simo et al. [1989]. Due to the symmetry properties, we can reduce the problem to one quarter of the plate with corresponding boundary conditions. Displacement controlled boundary conditions are imposed on the upper edge of the plate, see Figure 4.

Setup of BVP	
Left edge	$u_1 = 0$
Lower edge	$u_2 = 0$
Upper edge	$\boldsymbol{u} = (0, 6.15)^T \, \{\text{length}\}$
Young's modulus	$E = 70 \, \{\text{force}\}/\{\text{length}\}^2$
Poisson's ratio	$\nu = 0.2$
Yield stress	$y_0 = 0.243 \, \{\text{force}\}/\{\text{length}\}^2$
Hardening modulus	$h = 0.2 \, \{\text{force}\}/\{\text{length}\}^2$

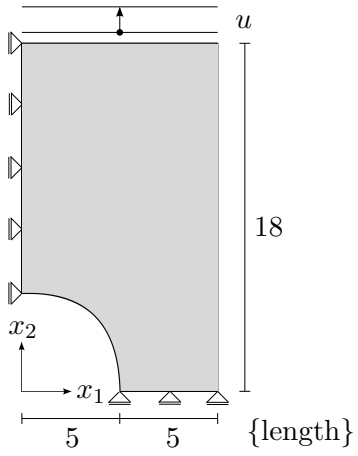

Figure 4: Geometrical and material setup for perforated plate problem

A load-displacement curve, where the corresponding load is calculated from the nodal reactions at the upper edge, is depicted in Figure 5. Here, we compare a standard displacement element, the mixed PHR formulation of Simo et al. [1989] and the proposed mixed PHR formulation each for a 72 and 722 element mesh. As depicted in the load-displacement curve, the results for the point- and element-wise enforcement of the return mapping algorithm for the PHR formulations and for the standard displacement formulation with the 722 element mesh show almost the same curve. Only the computation for the standard displacement formulation with the 72 element mesh results in a slightly different result. Additionally, the distribution of the equivalent plastic strains are given in Figure 8 for a Q1-, Q1P0- and the presented PHR element formulation, which are almost identical.

As a second aspect, we discuss the evolution of the plastic zone within the plate and the convergence rate of the energy norm for the global Newton iteration. We define the plastic

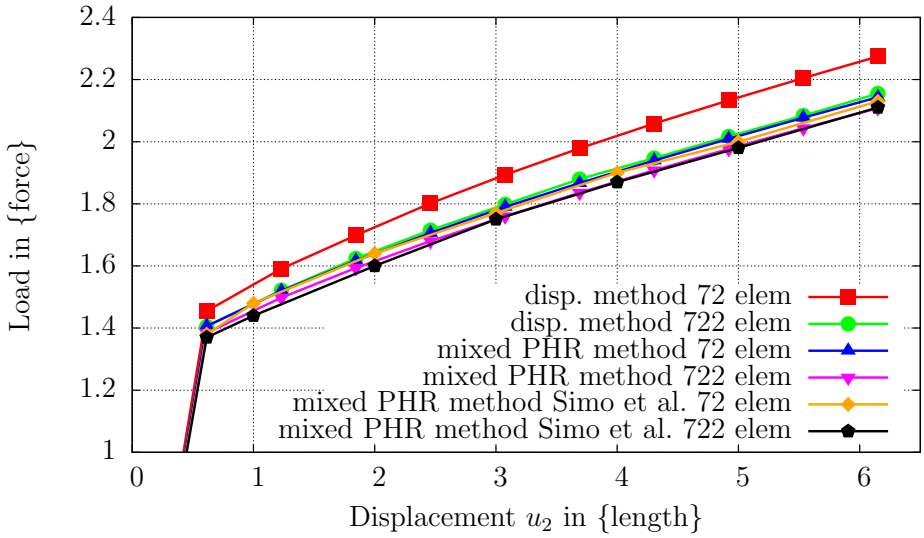

Figure 5: Load-displacement curves for perforated plate with 72 and 722 element meshes for displacement formulation, (element-wise enforcement of the flow rule) and proposed mixed PHR formulations (point-wise enforcement of the flow rule), see Simo et al. [1989]

zone for linear isotropic hardening as

$$\tilde{\phi} := ||\operatorname{dev} \boldsymbol{\sigma}|| / \sqrt{\frac{2}{3}} y_0 \,. \tag{56}$$

The plots determine three areas: a totally elastic region ($\tilde{\phi} < 0.9$), an elasto-plastic transition zone ($0.9 \leq \tilde{\phi} < 1.0$), where plasticity will occur in the case of continuous loading, and a completely plastic region ($\tilde{\phi} \geq 1.0$). Figure 6 and 7 illustrate the distribution of the plastic zone, which is given as an indicator for the plastic strains. The initial and maximum plastic strains occur at the stress concentration of the perforated plate, which is located at the right corner of the circular arc, (5,0).
The distribution of the plastic zone for both meshes is in a good agreement to the results given in Simo et al. [1989]. In addition, the rate of convergence for the Newton iteration for each formulation is given for both meshes. The chosen load steps are related to the one given in Simo et al. [1989]. For comparison of the convergence of the different approaches we introduce additionally the convergence rates for the mixed formulation taken from Simo et al. [1989], see Table 5 for the 72 element mesh and Table 6 for the 722 element mesh. The rates of convergence shown in Table 3 - 6 are satisfying due to the fact that quadratic convergence is attained only for energy norms below 10^{-6} caused by the radius of convergence. A second aspect is the slight degradation of the rate of convergence for more refined meshes. This degradation is shown for the mixed formulation in Table 4, e.g. for load step 10 the Newton method needs 11 iterations. The same effect is shown in Table 6 for the formulation of Simo et al. [1989], where load step 10 needs 10 Newton iterations.

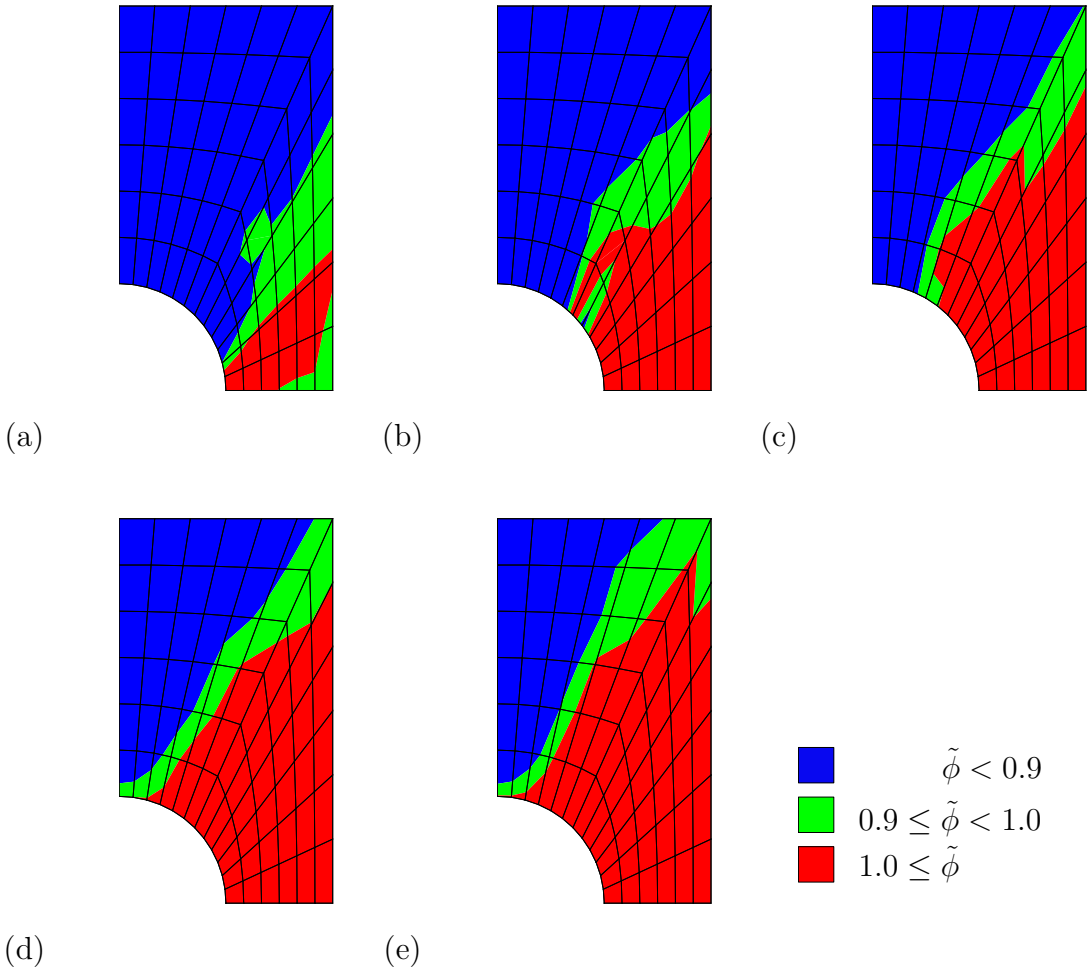

Figure 6: Distribution of $\tilde{\phi}$ for the proposed PHR formulation with point-wise enforcement of the flow rule on the undeformed 72 element mesh for a u_2 displacement of (a) 0.15, (b) 1.65, (c) 3.15, (d) 4.65 and (e) 6.15

	Load step			
	1	5	10	17
Iteration	($u_2 = 0.03$)	($u_2 = 0.15$)	($u_2 = 2.65$)	($u_2 = 6.15$)
1	1.0000e+00	1.0000e+00	1.0000e+00	1.0000e+00
2	4.3560e-03	6.7304e-03	1.2833e-03	6.0352e-04
3	2.1955e-02	1.4551e-02	5.8301e-03	1.2810e-03
4	2.6966e-02	2.0175e-03	4.4649e-04	6.9739e-04
5	1.2170e-03	5.1973e-06	8.5537e-04	2.0760e-05
6	1.2706e-03	8.4837e-10	6.4444e-06	5.0264e-08
7	9.5159e-06	3.2705e-15	1.8075e-09	9.6836e-13
8	8.7670e-09	-	2.1193e-15	-
9	1.2305e-15	-	-	-

Table 3: Global Newton iteration relative residual norm convergence rate for the presented point-wise PHR formulation considering a 72 element mesh

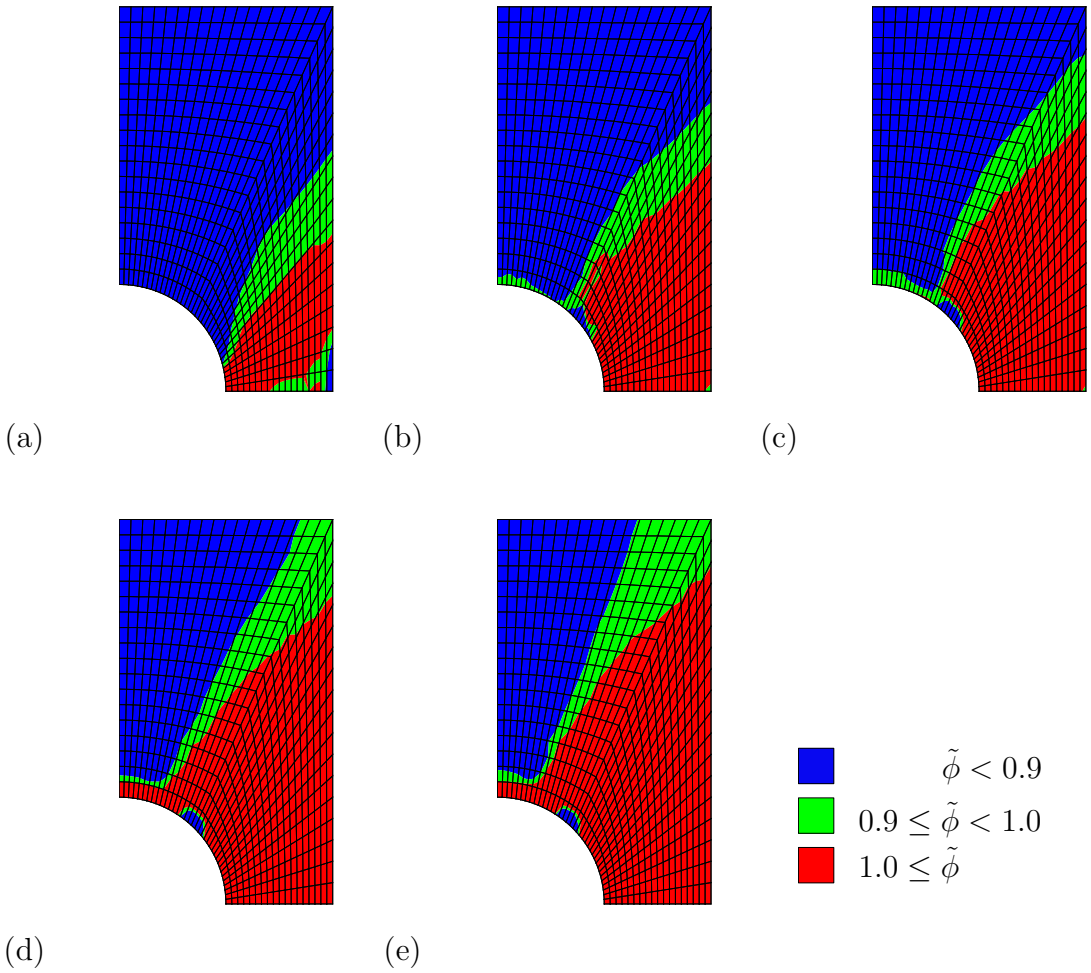

Figure 7: Distribution of $\tilde{\phi}$ for the proposed PHR formulation with point-wise enforcement of the flow rule on the undeformed 722 element mesh for a u_2 displacement of (a) 0.15, (b) 1.65, (c) 3.15, (d) 4.65 and (e) 6.15

	Load step			
	1	5	10	17
Iteration	($u_2 = 0.03$)	($u_2 = 0.15$)	($u_2 = 2.65$)	($u_2 = 6.15$)
1	1.0000e+00	1.0000e+00	1.0000e+00	1.0000e+00
2	1.1914e-03	2.4627e-03	1.0090e-03	2.3216e-04
3	4.5942e-02	1.1869e-02	4.0853e-03	9.3445e-04
4	1.6117e-03	6.8015e-04	1.2712e-03	6.9568e-04
5	3.1768e-04	1.0278e-03	9.0929e-04	1.8675e-04
6	2.5042e-06	1.6548e-05	1.3427e-04	3.9894e-05
7	2.4724e-08	9.5113e-08	9.4389e-05	6.9197e-06
8	1.8996e-14	9.7087e-14	5.6719e-06	1.1346e-05
9	-	-	6.7623e-06	7.6111e-09
10	-	-	3.3072e-09	2.4700e-13
11	-	-	8.0553e-15	-

Table 4: Global Newton iteration relative residual norm convergence rate for the presented point-wise PHR formulation considering a 722 element mesh

	Load step			
	1	5	10	17
Iteration	($u_2 = 0.03$)	($u_2 = 0.15$)	($u_2 = 2.65$)	($u_2 = 6.15$)
1	0.264e+00	0.288e+00	0.800e+02	0.779e+02
2	0.222e-04	0.164e-04	0.970e-03	0.196e-03
3	0.260e-04	0.165e-06	0.797e-04	0.139e-05
4	0.332e-08	0.645e-11	0.755e-06	0.278e-09
5	0.228e-14	0.956e-20	0.222e-09	0.210e-16
6	0.172e-26	0.116e-29	0.320e-16	0.564e-27

Table 5: Global Newton iteration energy norm convergence rate for the mixed formulation with element-wise enforcement of the flow rule taken from Simo et al. [1989] with 72 element mesh

	Load step			
	1	5	10	17
Iteration	($u_2 = 0.03$)	($u_2 = 0.15$)	($u_2 = 2.65$)	($u_2 = 6.15$)
1	0.897e+00	0.921e+00	0.256e+03	0.245e+03
2	0.220e-04	0.217e-04	0.831e-03	0.185e-03
3	0.175e-05	0.196e-05	0.683e-02	0.156e-04
4	0.449e-07	0.883e-07	0.753e-04	0.189e-05
5	0.320e-13	0.719e-10	0.871e-05	0.951e-07
6	0.559e-23	0.125e-15	0.275e-06	0.375e-11
7	-	0.483e-27	0.176e-07	0.210e-18
8	-	-	0.192e-11	0.164e-25
9	-	-	0.578e-19	-
10	-	-	0.255e-26	-

Table 6: Global Newton iteration energy norm convergence rate for the mixed formulation with element-wise enforcement of the flow rule taken from Simo et al. [1989] with 722 element mesh

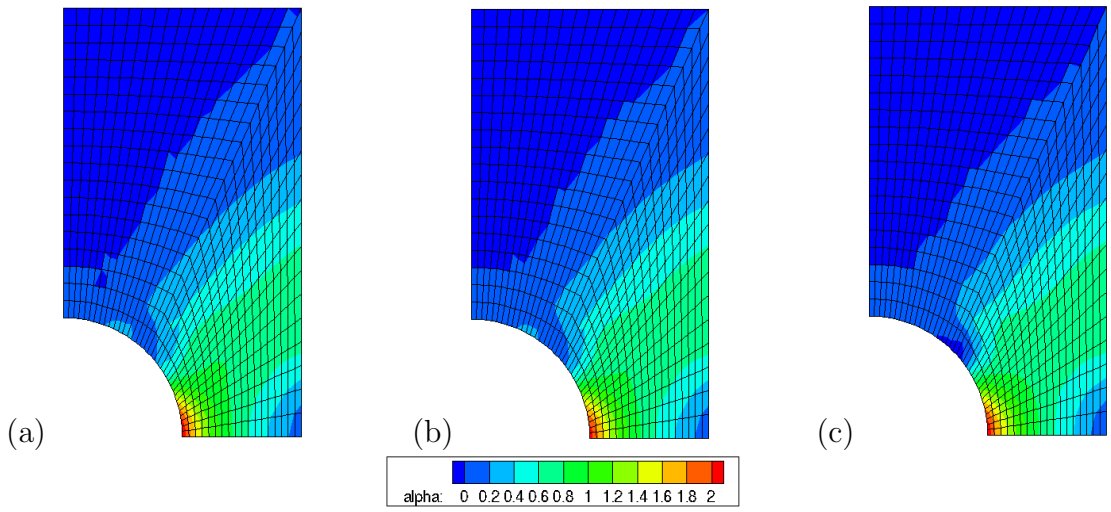

Figure 8: Distribution of equivalent plastic strains α for (a) the Q1, (b) the Q1P0 and (c) the presented PHR element formulation on the undeformed 722 element mesh under plane stress conditions for a u_2 displacement of 6.15

3.3. Elongation of a plate with circular inclusion - plane strain condition

A plate problem with an elastic circular inclusion is considered in order to demonstrate the performance of the plane strain algorithm within the presented PHR element formulation. Due to symmetry properties, only one quarter of the plate is investigated. The material setup and the geometry of the BVP is depicted in Figure 9. Here, the specimen is loaded by a displacement controlled boundary condition to a maximum of $u_2 = 0.1$mm.

Setup of BVP

Left edge	$u_1 = 0$
Lower edge	$u_2 = 0$
Upper edge	$\boldsymbol{u} = (0, 0.1)^T$ mm
Young's modulus	$E_1 = 206$ GPa
	$E_2 = 412$ GPa
Poisson's ratio	$\nu = 0.3$
Yield stress	$y_{01} = 1.0$ GPa
	$y_{02} \to \infty$
Hardening modulus	$h = 0.01$ GPa

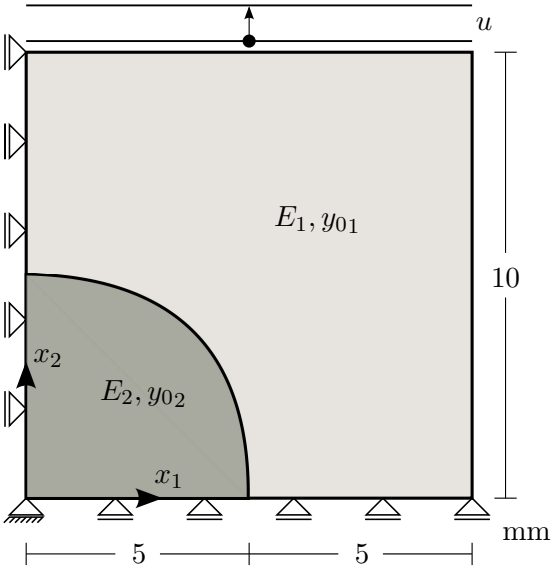

Figure 9: Geometrical and material setup for plate problem with circular inclusion

The load-displacement curve, where the corresponding load is calculated from the nodal reactions at the upper edge, in Figure 10 shows the comparison between the Q1, Q1P0 and the mixed PHR element for a 252 element mesh. Both mixed methods Q1P0 and PHR yield almost the same result, where the Q1 element shows an insignificant increase of load above a displacement of $u_2 = 0.7$mm.

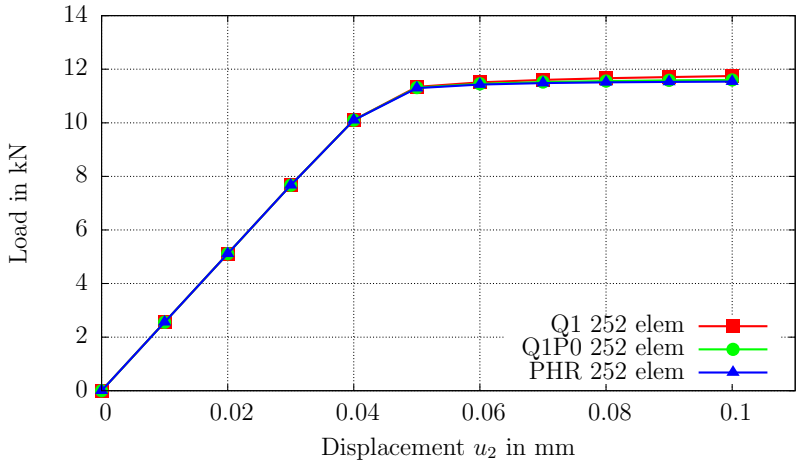

Figure 10: Load-displacement curves for the plate with inclusion under plane strain condition for a discretization with 252 elements for the Q1, Q1P0 and the proposed PHR element formulation

The distribution of the equivalent plastic strains at a top displacement of $u_2 = 0.05$mm, is depicted in Figure 11. The material response of the circular inclusion is purely elastic

and the plastic strains are concentrated above the purely elastic inclusion. The maximum amount of plastic strains occur above the top of the circular inclusion (0,5), which is given as the intersection of the elastic and elasto-plastic material. All element formulations yield a similar distribution of α where both mixed formulations Q1P0 and mixed PHR show a better agreement in the results for the region of maximum plastic strains compared to the standard Galerkin element formulation. Additionally, the distribution of the stresses

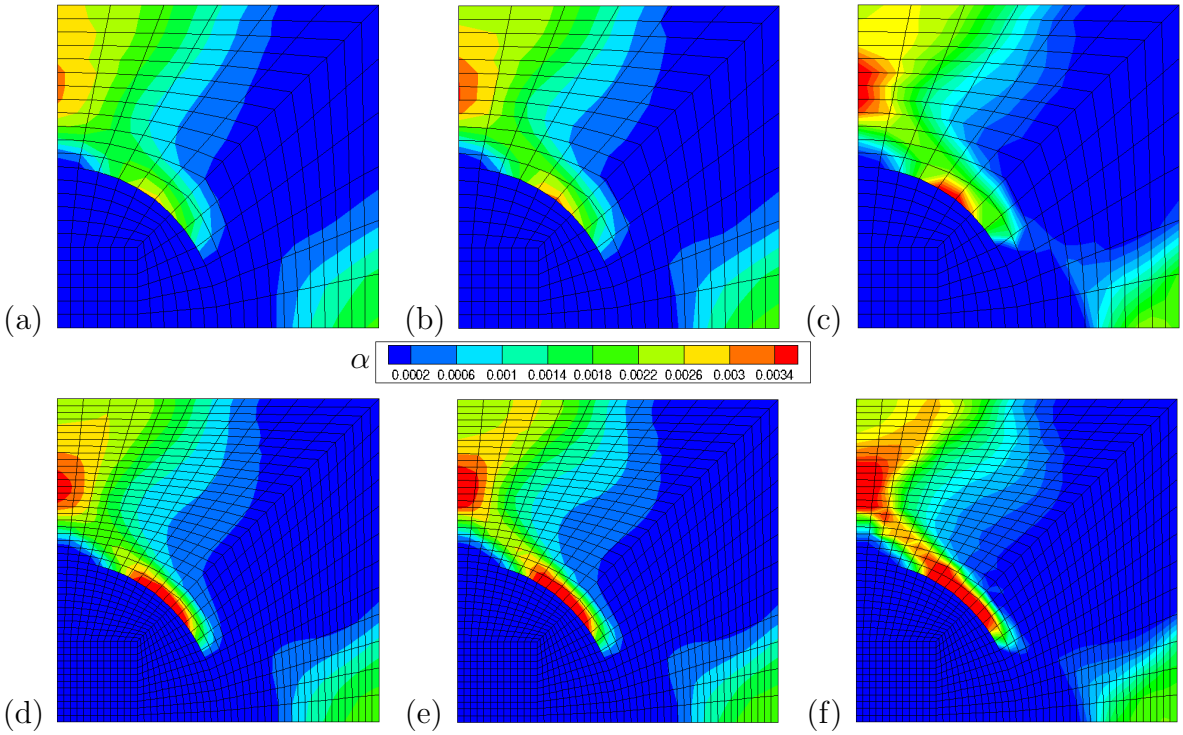

Figure 11: Plane strain condition. Distribution of equivalent plastic strains α for Q1 (a), (d), Q1P0 (b), (e) and PHR (c), (f) element for a top displacement of 0.05 mm (upper row, discretization with 252 elements; lower row, discretization with 1008 elements)

σ_{11}, σ_{33} and the plastic strains ε^p_{33} for the standard Galerkin Q1, the mixed Q1P0 and the mixed PHR element formulation are depicted in Figure 12 - 14. The results for all formulations yield similar behavior due to loading and are in good agreement.

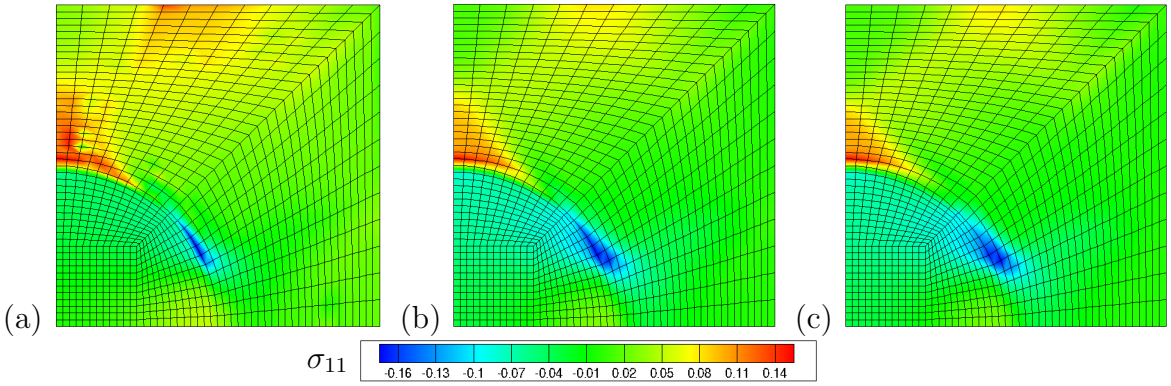

Figure 12: Plane strain condition. Distribution of σ_{11} for Q1 (a), Q1P0 (b) and PHR (c) formulation on the undeformed 1008 element mesh for a top displacement of $u_2 = 0.05$ mm

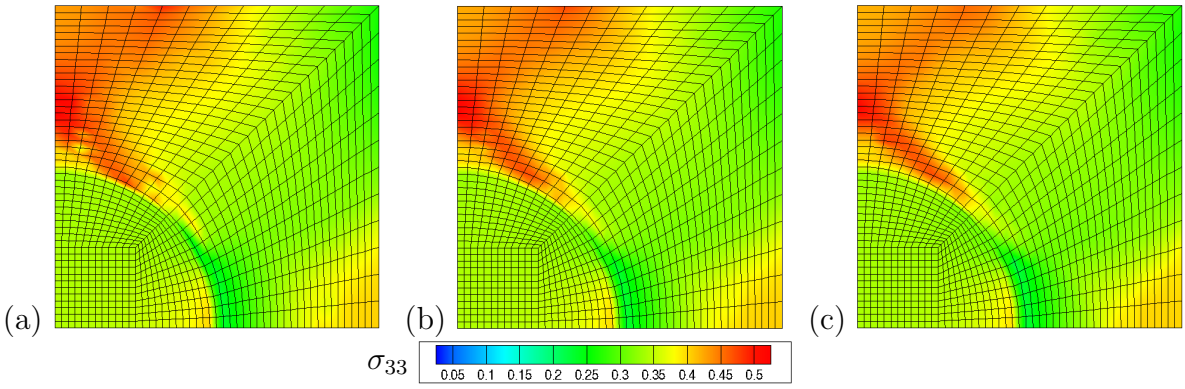

Figure 13: Plane strain condition. Distribution of σ_{33} for Q1 (a), Q1P0 (b) and PHR (c) formulation on the undeformed 1008 element mesh for a top displacement of $u_2 = 0.05$ mm

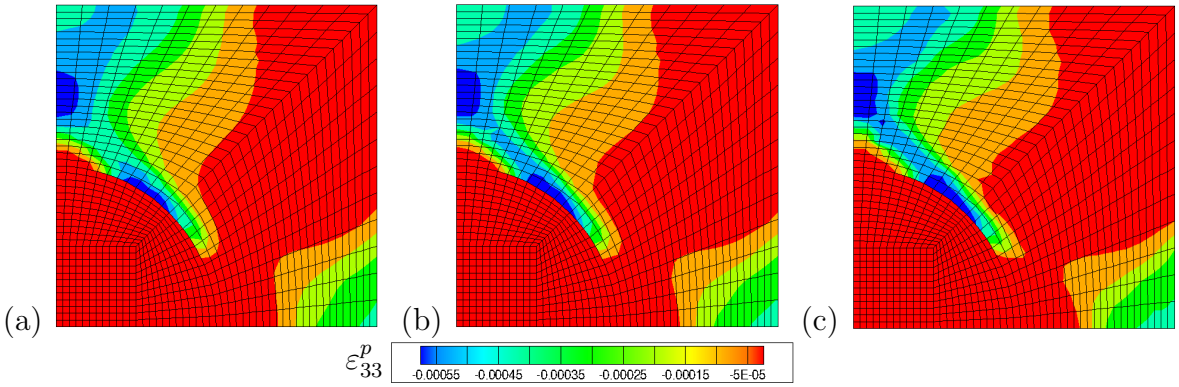

Figure 14: Plane strain condition. Distribution of ε^p_{33} for Q1 (a), Q1P0 (b) and PHR (c) formulation on the undeformed 1008 element mesh for a top displacement of $u_2 = 0.05$ mm

Additionally, Table 7 shows the convergence of the relative residual norm of the plane strain algorithm.

	Load step	
	20	20
Iteration	($u_2 = 0.1$)	($u_2 = 0.1$)
1	1.000e+00	1.000e+00
2	1.097e-04	1.097e-04
3	3.386e-05	3.386e-05
4	1.284e-06	1.284e-06
5	3.004e-09	3.004e-09
6	1.206e-11	1.710e-10
7	-	1.451e-11

Table 7: Global Newton iteration relative residual norm convergence rate for the mixed formulation with point-wise enforcement of the flow rule with 252 (left) and 1008 (right) element mesh under plane strain condition

4. Concluding remarks

We proposed a mixed finite element formulation based on the Prange-Hellinger-Reissner principle for small strain elasto-plasticity including linear isotropic hardening. An independent stress interpolation is realized with the discontinuous 5-parameter approach by Pian and Sumihara [1984]. In order to increase efficiency, a static condensation of the stress field with respect to the displacements is performed.
Comparing the presented simulations of Cook's membrane problem and the perforated plate, we conclude that the proposed PHR formulation based on a point-wise enforcement of the flow rule are in good agreement with the approach of Simo et al. [1989], with an element-wise enforcement of the flow rule. This is also depicted in the convergence study for Cook's membrane where the proposed mixed PHR formulation is in the range of the convergence rate of the mixed PHR formulation from Simo et al. [1989].

Acknowledgement

The authors gratefully acknowledge the support by the Deutsche Forschungsgemeinschaft in the Priority Program 1748 "Reliable simulation techniques in solid mechanics. Development of non- standard discretization methods, mechanical and mathematical analysis" under the project "First-order system least squares finite elements for finite elasto-plasticity" (SCHR 570/24-1, SCHW 1355/2-1 and STA 402/12-1). Furthermore, we thank B.D. Reddy and P. Wriggers for their helpful remarks and discussions on the subject of this paper.

References

D. N. Arnold and R. Winther. Nonconforming mixed elements for elasticity. *Math. Models Meth. Appl. Sci.*, 13:295–307, 2003.

D. N. Arnold, F. Brezzi, and J. Douglas. PEERS: A new mixed finite element for plane elasticity. *Japan J. Appl. Math.*, 1:347–367, 1984.

D. N. Arnold, R. S. Falk, and R. Winther. Mixed Finite Element Methods for Linear Elasticity with Weakly Imposed Symmetry. *Math. Comp.*, 76:1699–1723, 2007.

F. Auricchio, F. Brezzi, and C. Lovadina. *Encyclopedia of Computational Mechanics*. John Wiley & Sons, Ltd., 2 edition, 2004.

I. Babuška. The finite element method with Lagrangian multipliers. 20(3):179–192, 1973.

D. Boffi, F. Brezzi, and M. Fortin. Reduced Symmetry Elements in Linear Elasticity. *Commun. Pure Appl. Anal.*, 8:95–121, 2009.

D. Boffi, F. Brezzi, and M. Fortin. *Mixed Finite Element Methods and Applications*. Springer, Heidelberg, 2013.

F. Brezzi. On the existence, uniqueness and approximation of saddle-point problems arising from Lagrangian multipliers. 8(2):129–151, 1974.

F. Brezzi, J. Douglas, and L. D. Marini. Two families of mixed finite elements for second order elliptic problems. *Numer. Math.*, 47:217–235, 1985.

K.S. Chun, S.K. Kassenge, and W.T. Park. Static assessment of quadratic hybrid plane stress element using non-conforming displacement modes and modified shape functions. *Structural Engineering and Mechanics*, 29:643–658, 2008.

B. Cockburn, J. Gopalakrishnan, and J. Guzmán. A New Elasticity Element Made For Enforcing Weak Stress Symmetry. *Math. Comp.*, 79:1331–1349, 2010.

R.D. Cook. Improved two-dimensional finite element. *Journal of Structural Division*, 100 (9):1851–1863, September 1974.

R. De Borst. The zero-normal-stress condition in plane-stress and shell elastoplasticity. *Communications in Applied Numerical Methods*, 7:29–33, 1991.

B.M. Fraeijs de Veubeke. Diffusion des inconnues hyperstatiques dans les voilures á longeron couplès. *Bull. Serv. Technique de L'Aéronautique, Imprimeríe Marcel Hayez, Bruxelles*, No. 24:56pp, 1951.

B.G. Galerkin. Series solution of some problems in elastic equilibrium of rods and plates. *Vestn. Inzh. Tech.*, 19:897–908, 1915.

W. Han and B.D. Reddy. On the finite element method for mixed variational inequalities arising in elastoplasticity. *SIAM Journal on Numerical Analysis*, 32:1778–1807, 1995.

E. Hellinger. *Encyklopädie der mathematischen Wissenschaften mit Einschluss ihrer Anwendungen*, volume 4, chapter Die allgemeine Ansätze der Mechanik der Kontinua. 1914.

H.-C. Hu. On some variational methods on the theory of elasticity and the theory of plasticity. *Scientia Sinica*, Vol. 4:33–54, 1955.

O. Klaas, J. Schröder, E. Stein, and C. Miehe. A regularized dual mixed element for plane elasticity implementation and performance of the BDM element. *Computer Methods in Applied Mechanics and Engineering*, 121:201–209, 1995.

S.O. Klinkel and S. Govindjee. Using finite strain 3D-material models in beam and shell elements. *Engineering Computations*, 19(3):254–271, 2002.

O. Ladyzhenskaya. *The mathematical theory of viscous incompressible flow*, volume 76. Gordon and Breach New York, 1969.

M. Lonsing and R. Verfürth. On the stability of BDMS and PEERS elements. *Numer. Math.*, 99:131–140, 2004.

T.H.H. Pian and K. Sumihara. A Rational Approach for Assumed Stress Finite Elements. *Int. J. Numer. Meth. Engng.*, 20:1685–1695, 1984.

G. Prange. *Das Extremum der Formänderungsarbeit.* Habilitationsschrift, Technische Hochschule Hannover, 1916.

B.D. Reddy. Mixed variational inequalities arising in elastoplasticity. *Nonlinear Analysis*, 19:1071–1089, 1992.

E. Reissner. On a variational theorem in elastictiy. *J. Math. Phys.*, Vol. 29:90–95, 1950.

J. Schröder, O. Klaas, E. Stein, and C. Miehe. A physically nonlinear dual mixed finite element formulation. *Computer Methods in Applied Mechanics and Engineering*, 144: 77–92, 1997.

J. C. Simo. Numerical Analysis and Simulation of Plasticity. In P. G. Ciarlet and J. L. Lions, editors, *Handbook of Numerical Analysis*, volume VI, pages 183–499. 1998.

J.C. Simo. A framework for finite strain elastoplasticity based on maximum plastic dissipation and the multiplicative decomposition: Part I. Continuum formulation. 66: 199–219, 1988a.

J.C. Simo. A framework for finite strain elastoplasticity based on maximum plastic dissipation and the multiplicative decomposition. Part II: Computational aspects. 68:1–31, 1988b.

J.C. Simo and T.J.R. Hughes. *Computational Inelasticity.* Springer-Verlag, New York, 1998.

J.C. Simo, J.G. Kennedy, and R.L. Taylor. Complementary mixed finite element formulations for elastoplasticity. *Computer Methods in Applied Mechanics and Engineering*, 74:177–206, 1989.

E. Stein and F.-J. Barthold. *Elastizitätstheorie.* Ernst & Sohn, Berlin, 1996.

R. Stenberg. A Family of Mixed Finite Elements for the Elasticity Problem. *Numer. Math.*, 53:513–538, 1988.

K. Washizu. On the variational principles of elasticity and plasticity. *Aeroelastic and Structure Research Laboratory, Technical Report 25-18, MIT, Cambridge*, 1955.

M.L. Wilkins. Calculation of elastic-plastic flow. In B. Adler, S. Fernback, and M. Rotenberg, editors, *Methods of Computational Physics*, volume 3, pages 211–272. Academic Press, New York, 1964.

P. Wriggers and J. Korelc. On enhanced strain methods for small and finite deformations of solids. *Computational Mechanics*, 18:413–428, 1996.

A Appendix

The definitions for the approximation matrices for displacements $\underline{\boldsymbol{N}}$ and $\underline{\boldsymbol{B}}$ as well as the interpolation matrices related to the stresses $\underline{\boldsymbol{S}}$ are

$$\underline{\boldsymbol{B}}^I = \begin{bmatrix} N^I_{,1} & 0 \\ 0 & N^I_{,2} \\ N^I_{,2} & N^I_{,1} \end{bmatrix}, \quad \underline{\boldsymbol{N}}^I = \begin{bmatrix} N^I & 0 \\ 0 & N^I \end{bmatrix} \quad \text{and} \quad \underline{\boldsymbol{S}}^J = \begin{bmatrix} 1 & 0 & 0 & a_1^2\eta & a_3^2\xi \\ 0 & 1 & 0 & b_1^2\eta & b_3^2\xi \\ 0 & 0 & 1 & a_1b_1\eta & a_3b_3\xi \end{bmatrix} \tag{57}$$

where a_i and b_i with $i = 1, 2, 3$ are given from the Jacobian matrix for the undeformed quadrilateral reference element given in Pian and Sumihara [1984] as

$$\boldsymbol{J} = \begin{bmatrix} J_{11} & J_{12} \\ J_{21} & J_{22} \end{bmatrix} = \begin{bmatrix} \frac{\partial x}{\partial \xi} & \frac{\partial y}{\partial \xi} \\ \frac{\partial x}{\partial \eta} & \frac{\partial y}{\partial \eta} \end{bmatrix} = \begin{bmatrix} a_1 + a_2\eta & b_1 + b_2\eta \\ a_3 + a_2\xi & b_3 + b_2\xi \end{bmatrix} \tag{58}$$

$$\begin{aligned} a_1 &= \tfrac{1}{4}(-x_1 + x_2 + x_3 - x_4) \\ a_2 &= \tfrac{1}{4}(x_1 - x_2 + x_3 - x_4) \\ a_3 &= \tfrac{1}{4}(-x_1 - x_2 + x_3 + x_4) \\ b_1 &= \tfrac{1}{4}(-y_1 + y_2 + y_3 - y_4) \\ b_2 &= \tfrac{1}{4}(y_1 - y_2 + y_3 - y_4) \\ b_3 &= \tfrac{1}{4}(-y_1 - y_2 + y_3 + y_4) \end{aligned} \tag{59}$$

Regarding the reference quadrilateral element with the coordinates (-1,-1), (1,-1), (1,1) and (-1,1), the interpolation matrix $\underline{\boldsymbol{S}}$ reduces to

$$\underline{\boldsymbol{S}}^J = \begin{bmatrix} 1 & 0 & 0 & \eta & 0 \\ 0 & 1 & 0 & 0 & \xi \\ 0 & 0 & 1 & 0 & 0 \end{bmatrix} \tag{60}$$

The fourth-order compliance tensor $\mathbb{C}^{-1}$ for determining the overall material tangent $\mathbb{D}^{ep} = \mathbb{C}^{-1} + \partial_\sigma \boldsymbol{\varepsilon}^p$ and the elastic strain tensor in matrix notation $\underline{\boldsymbol{\varepsilon}}^e = \underline{\mathbb{C}}^{-1} : \underline{\boldsymbol{\sigma}}$ is defined for linear elasticity in Stein and Barthold [1996] as

$$\begin{pmatrix} \varepsilon_{11} \\ \varepsilon_{22} \\ \varepsilon_{33} \\ 2\varepsilon_{12} \\ 2\varepsilon_{23} \\ 2\varepsilon_{13} \end{pmatrix} = \tfrac{1}{E} \begin{pmatrix} 1 & -\nu & -\nu & 0 & 0 & 0 \\ -\nu & 1 & -\nu & 0 & 0 & 0 \\ -\nu & -\nu & 1 & 0 & 0 & 0 \\ 0 & 0 & 0 & 2(1+\nu) & 0 & 0 \\ 0 & 0 & 0 & 0 & 2(1+\nu) & 0 \\ 0 & 0 & 0 & 0 & 0 & 2(1+\nu) \end{pmatrix} \begin{pmatrix} \sigma_{11} \\ \sigma_{22} \\ \sigma_{33} \\ \sigma_{12} \\ \sigma_{23} \\ \sigma_{13} \end{pmatrix} . \tag{61}$$